

Electrodeposited Aluminum-Doped α -Fe₂O₃ Photoelectrodes: Experiment and Theory

Alan Kleiman-Shwarscstein,^{†,§} Muhammad N. Huda,^{||} Aron Walsh,^{||} Yanfa Yan,^{||}
Galen D. Stucky,^{†,‡} Yong-Sheng Hu,^{*,§,†} Mowafak M. Al-Jassim,^{||} and
Eric W. McFarland^{*,§}

[†]Materials Department, University of California, Santa Barbara, California 93106,

[‡]Department of Chemistry and Biochemistry, University of California, Santa Barbara,

California 93106, [§]Department of Chemical Engineering, University of California, Santa Barbara,
California 93106, ^{||}Beijing National Laboratory for Condensed Matter Physics, Institute of Physics,
Chinese Academy of Sciences, Beijing 100190, China, and ^{||}National Renewable Energy Laboratory,
Golden, Colorado 80401

Received October 11, 2009. Revised Manuscript Received November 30, 2009

Substitutional doping can improve the electronic properties of α -Fe₂O₃ for the solar photoelectrochemical (PEC) applications. Generally speaking, nonisovalent substitutional doping helps to enhance the electronic conductivity of α -Fe₂O₃. However, we found that the introduction of strain in the lattice, which is achieved by isovalent substitutional doping of an Al, can also improve the electronic properties. α -Fe₂O₃ films with the Al dopant atomic concentration varying from 0 to 10% were prepared by electrodeposition, and their performance for photoelectrochemical hydrogen production was characterized. Results indicate that the incident photon conversion efficiency (IPCE) for ~0.45 at-% Al substitution increases by 2- to 3-fold over undoped samples. Density-functional theory (DFT) was utilized to interpret the experimental findings. It was shown that although no substantial change to the electronic structure, a contraction of the crystal lattice due to the isovalent replacement of Fe³⁺ by an Al³⁺ benefits the small polaron migration, resulting in an improvement in conductivity compared to the undoped samples.

1. Introduction

Although the concept of solar-to-chemical energy conversion using semiconductor-based photoelectrochemical processes has been explored for decades,^{1–5} a cost-effective solar sensitive material system for water splitting, or any chemical process, has not been identified in the last 30 years after the first report of photoelectrochemical hydrogen production on TiO₂.⁶ The requirements of such a material are well-known, and the phenomena are fundamentally understood. The challenge is in the discovery of a cost-effective and electrolyte-stable semiconductor material that has (a) a bandgap energy sufficient to provide the required electrosynthetic reaction overpotential (~1.6 eV for water splitting), (b) a conduction band edge that is higher in energy than the required cathodic overpotential, (c) a valence band edge that is lower in energy than the required anodic overpotential, (d) high rates of charge separation and transfer

to electrochemical products relative to the carrier recombination rate, and (e) material stability with lifetimes of the photocatalyst for thousands of hours.

Hematite (α -Fe₂O₃) has long been of interest as a potential photoelectrochemical material because it is one of the most abundant and inexpensive semiconductors on earth with a bandgap (~2.1 eV) that is energetically appropriate for water splitting. Hematite is stable in most electrolytes at pH > 3 and it is nontoxic. Unfortunately, pure-phase hematite is a charge transfer-type Mott insulator with intrinsically poor conductivity^{7,8} (by small polarons⁹) which limits the quantum efficiency for any photoelectrochemical process. Furthermore, hematite has anisotropic conductivity with approximately 4 orders of magnitude higher conductivity in the [110] plane compared to the orthogonal plane.^{10,11} For water photoelectrolysis to make hydrogen, hematite is further limited by the energy of the conduction band relative to the redox level of the H₂/H⁺ couple (~0.2 V vs NHE) and low electrocatalytic rates of oxygen evolution on the oxide surface.

- *Authors to whom correspondence should be addressed: E-mail: yshu@aphy.iphy.ac.cn (Y.S-H.) mcfar@engineering.ucsb.edu (E.W.M.).
(1) Khaslev, O.; Turner, J. A. *Science* **1998**, *280*, 425.
(2) Zou, Z. G.; Ye, J. H.; Sayama, K.; Arakawa, H. *Nature* **2001**, *414*, 625.
(3) Gratzel, M. *Nature* **2001**, *414*, 338.
(4) Maeda, K.; Teramura, K.; Lu, D. L.; Takata, T.; Saito, N.; Inoue, Y.; Domen, K. *Nature* **2006**, *440*, 295.
(5) Wang, X. C.; Maeda, K.; Thomas, A.; Takanabe, K.; Xin, G.; Carlsson, J. M.; Domen, K.; Antonietti, M. *Nat. Mater.* **2009**, *8*, 76.
(6) Fujishima, A.; Honda, K. *Nature* **1972**, *238*, 37.

- (7) Fujimori, A.; Saeki, M.; Kimizuka, N.; Taniguchi, M.; Suga, S. *Phys. Rev. B* **1986**, *34*, 7318.
(8) Morin, F. J. *Phys. Rev.* **1951**, *83*, 1005.
(9) Kerisit, S.; Rosso, K. M. *J. Chem. Phys.* **2007**, *127*.
(10) Iordanova, N.; Dupuis, M.; Rosso, K. M. *J. Chem. Phys.* **2005**, *122*.
(11) Kay, A.; Cesar, I.; Gratzel, M. *J. Am. Chem. Soc.* **2006**, *128*, 15714.

To improve upon hematite's intrinsic electronic properties substitutitional doping with Si,^{11–13} Ti,^{8,12,14,15} Pt, Mo, Cr,¹⁶ Zn,^{17,18} and Ge¹² among other atoms has been reported. Methods such as electrodeposition,^{16,19–23} spray pyrolysis,^{24–27} sol–gel,^{28–32} and chemical vapor deposition processes^{11,33–35} among others have been used to synthesize doped iron oxide. In most cases any improvement in performance has been attributed to improved conductivity due to a preferential ordering of the crystallites or lattice distortions which change the structural symmetries and relax the constraint on spin-forbidden transitions from the undoped Mott Insulator. The electron transport properties of hematite may also be improved by introducing strain into the lattice by the application of pressure. Hematite undergoes a phase transition at 40–50 GPa^{36,37} which induces a breakdown of the d-electron correlation collapsing the magnetic ordering and the onset of an insulator-to-metal transition due to the closing of the d–d or p–d gap. Although it is impractical to operate photocatalysts at high pressures and the material's opto-electronic properties after the phase transition may be undesirable, smaller strains to the lattice induced by substitutional doping can decrease the Fe—O—Fe bond distance in the ferromagnetically coupled hematite bilayer, along the (001) basal plane.

- (12) Kennedy, J. H.; Anderman, M.; Shinar, R. *J. Electrochem. Soc.* **1981**, *128*, 2371.
 (13) Leygraf, C.; Hendewerk, M.; Somorjai, G. A. *J. Phys. Chem.* **1982**, *86*, 4484.
 (14) Glasscock, J. A.; Barnes, P. R. F.; Plumb, I. C.; Savvides, N. *J. Phys. Chem. C* **2007**, *111*, 16477.
 (15) Hu, Y. S.; Kleiman-Shwarscstein, A.; Stucky, G. D.; McFarland, E. W. *Chem. Commun.* **2009**, 2652.
 (16) Hu, Y. S.; Kleiman-Shwarscstein, A.; Forman, A. J.; Hazen, D.; Park, J. N.; McFarland, E. W. *Chem. Mater.* **2008**, *20*, 3803.
 (17) Ingler, W. B.; Baltrus, J. P.; Khan, S. U. M. *J. Am. Chem. Soc.* **2004**, *126*, 10238.
 (18) Kumari, S.; Tripathi, C.; Singh, A. P.; Chauhan, D.; Shrivastav, R.; Dass, S.; Satsangi, V. R. *Curr. Sci.* **2006**, *91*, 1062.
 (19) Kleiman-Shwarscstein, A.; Hu, Y. S.; Forman, A. J.; Stucky, G. D.; McFarland, E. W. *J. Phys. Chem. C* **2008**, *112*, 15900.
 (20) Spray, R. L.; Choi, K. S. *Chem. Mater.* **2009**, *21*, 3701.
 (21) Prakasam, H. E.; Varghese, O. K.; Paulose, M.; Mor, G. K.; Grimes, C. A. *Nanotechnology* **2006**, *17*, 4285.
 (22) Mohapatra, S. K.; Banerjee, S.; Misra, M. *Nanotechnology* **2008**, *19*.
 (23) Tahir, A. A.; Wijayantha, K. G. U.; Saremi-Yarahmadi, S.; Mazhar, M.; McKee, V. *Chem. Mater.* **2009**, *21*, 3763.
 (24) Kumari, S.; Singh, A. P.; Tripathi, C.; Chauhan, D.; Dass, S.; Shrivastav, R.; Gupta, V.; Sreenivas, K.; Satsangi, V. R. *Int. J. Photoenergy* **2007**.
 (25) Sartoretti, C. J.; Alexander, B. D.; Solarska, R.; Rutkowska, W. A.; Augustynski, J.; Cerny, R. *J. Phys. Chem. B* **2005**, *109*, 13685.
 (26) Ingler, W. B.; Khan, S. U. M. *Int. J. Hydrogen Energy* **2005**, *30*, 821.
 (27) Khan, S. U. M.; Akikusa, J. *J. Phys. Chem. B* **1999**, *103*, 7184.
 (28) Zhan, S. H.; Chen, D. R.; Jiao, X. L.; Liu, S. S. J. *Colloid Interface Sci.* **2007**, *308*, 265.
 (29) Avila-Garcia, A.; Carbajal-Franco, G.; Tiburcio-Silver, A.; Barrera-Calva, E.; Andrade-Ibarra, E. *Rev. Mex. Fis.* **2003**, *49*, 219.
 (30) Watanabe, A.; Kozuka, H. *J. Phys. Chem. B* **2003**, *107*, 12713.
 (31) Long, J. W.; Logan, M. S.; Rhodes, C. P.; Carpenter, E. E.; Stroud, R. M.; Rolison, D. R. *J. Am. Chem. Soc.* **2004**, *126*, 16879.
 (32) Woo, K.; Lee, H. J.; Ahn, J. P.; Park, Y. S. *Adv. Mater.* **2003**, *15*, 1761.
 (33) Cesar, I.; Sivula, K.; Kay, A.; Zboril, R.; Graetzel, M. *J. Phys. Chem. C* **2009**, *113*, 772.
 (34) Saremi-Yarahmadi, S.; Wijayantha, K. G. U.; Tahir, A. A.; Vaidhyananthan, B. *J. Phys. Chem. C* **2009**, *113*, 4768.
 (35) Sivula, K.; Le Formal, F.; Gratzel, M. *Chem. Mater.* **2009**, *21*, 2862.
 (36) Olsen, J. S.; Cousins, C. S. G.; Gerward, L.; Jhans, H.; Sheldon, B. *J. Phys. Scr.* **1991**, *43*, 327.
 (37) Rozenberg, G. K.; Dubrovinsky, L. S.; Pasternak, M. P.; Naaman, O.; Le Bihan, T.; Ahuja, R. *Phys. Rev. B* **2002**, *65*.
 (38) Zoppi, A.; Lofrumento, C.; Castellucci, E. M.; Sciau, P. *J. Raman Spectrosc.* **2008**, *39*, 40.
 (39) Stanjek, H.; Schwertmann, U. *Clays Clay Miner.* **1992**, *40*, 347.
 (40) Rosso, K. M.; Smith, D. M. A.; Dupuis, M. *J. Chem. Phys.* **2003**, *118*, 6455.
 (41) Velev, J.; Bandyopadhyay, A.; Butler, W. H.; Sarker, S. *Phys. Rev. B* **2005**, *71*.
 (42) Droubay, T.; Rosso, K. M.; Heald, S. M.; McCready, D. E.; Wang, C. M.; Chambers, S. A. *Phys. Rev. B* **2007**, *75*.

Such strain is expected to increase conductivity^{38,39} By substituting an Fe atom with a cation having a smaller size such as Al or B, this will decrease the Fe—O—metal bond distance and mimic the effects of pressure on the lattice.

Band structure calculations by first principle density functional theory (DFT) to better understand the conduction properties of pure α -Fe₂O₃ have been performed by Rosso et al.^{10,40} For applications to magnetic materials, metal-doped α -Fe₂O₃ ($M = \text{Sc}, \text{Ti}, \text{V}, \text{Cr}, \text{Mn}, \text{Fe}, \text{Co}, \text{Ni}, \text{Cu}, \text{Zn}, \text{Ga}$) has been investigated,⁴¹ and Ti doped iron oxide was studied theoretically and experimentally by Droubay for its magnetism and conductivity properties.⁴²

In this work we combine experimental and theoretical work to explore the isovalent replacement of Fe³⁺ by Al³⁺. This report addresses the following questions relevant to doped iron oxide photocatalysts: (1) Can isovalent substitution of iron by aluminum improve the electron/hole transport properties of hematite photoelectrodes? (2) Is there an optimal concentration of aluminum in hematite for maximum PEC performance? (3) How do the observed performance trends correlate to theoretical predictions?

2. Experimental Section

Electrodeposition of Thin Films. Electrodeposition of undoped and aluminum-doped films was performed using a three-electrode configuration, a Pt mesh, Ag/AgCl saturated by KCl, and a platinized quartz substrate in which a Ti adhesion layer (50 nm) is deposited on the quartz followed by a 150 nm Pt layer or a fluorine-doped tin oxide (FTO, TEC 15, Pilkington glass) was used as counter, reference, and working electrodes, respectively. The electrodeposition solution¹⁹ consisted of 5 mM FeCl₃ + 5 mM KF + 0.1 M KCl + 1 M H₂O₂; the aluminum doping was achieved by varying the atomic concentrations (Al/(Al+Fe)) by addition of an aqueous stock solution of AlCl₃. The Al molar ratios in the electrolyte ranged from 0% to 40%. The deposition of the films was performed by cyclic voltammetry with the applied voltage scanned between –0.49 and 0.41 V vs Ag/AgCl at a rate of 0.2 V/sec. For the electrodes grown on Pt/Ti coated quartz wafers, five cycles were enough to deposit an appreciable amount of iron hydroxide ($\sim 0.7 \pm 0.2 \mu\text{m}$) while in the case of the FTO substrates 50 cycles were used for depositing samples for XRD and UV-vis measurements. After electrodeposition, the films were washed with DI water three times to remove any residual electrolyte followed by calcination in air at 700 °C for the Pt/Ti substrate and 600 °C for the FTO substrate with a heating rate of 2 °C/min and a dwell time of 4 h for all samples.

Sample Characterization. Inductively coupled argon plasma (ICP, Thermo iCAP 6300 inductively coupled plasma spectrometer) was used to determine the aluminum to iron ratio of the

electrodeposited films; all dopant percentages reported herein are those measured by ICP in the film and not those of the electrodeposition solution unless indicated otherwise. The atomic % in the film percentages was used throughout the manuscript to identify the samples. Samples were deposited on a Pt foil that was cleaned prior to sample deposition by electrochemically etching in 1 M HNO₃, and afterward samples were washed with DI water and dried under nitrogen stream. The same electrodeposition conditions were used as the quartz/Ti/Pt substrates but in this case 10 cyclic voltammograms were performed to increase the deposition thickness. After deposition the samples were rinsed with DI water, dried under nitrogen, and dissolved in 10% HCl (Fisher Chemical, TraceMetal grade). To reduce any aluminum cross-contamination, care was taken to avoid any glass-containing materials during the preparation of the calibration standards and dissolution of the films. Calibration standards for ICP were prepared from a 1 mg/mL stock solutions of Fe and Al (High Purity Standards) stabilized in 2% HNO₃ and diluted using 10% HCl solution. X-ray diffraction (XRD) was performed on FTO samples rather than on the platinum electrodes using a powder diffractometer in a grazing incidence configuration $\theta = 0.5^\circ$ (Phillips PANalytical X'PERT, using Cu K α radiation). The XRD measurements were obtained on FTO because it is less crystalline than the Pt/Ti electrodes and resulted in higher quality XRD spectra. Scanning electron microscopy (SEM) was performed on the aluminum-doped hematite samples with an acceleration voltage of 5 KeV and a working distance of ~ 5 mm from the tip to the sample plane (FEI Co. XL 40; UHR mode). UV-vis spectroscopy of the electrodeposited samples on FTO was performed using a Shimadzu UV3600 UV-NIR Spectrometer with an integrating sphere in transmission mode.

Photoelectrochemical Performance. The photoelectrochemical measurements^{43,44} of the samples were tested in a three electrode configuration with a Pt counter electrode, KCl saturated Ag/AgCl reference electrode and the hematite sample as the working electrode; details of the experimental setup have been previously published.¹⁹ The electrolyte consisted of a N₂ degassed 1 M solution of NaOH in DI water (Milli-Q, Millipore Corp.; 18.2 M Ω) at pH 13.6, which was continuously degassed with N₂ (to decrease the oxygen reduction reaction at the counter electrode). Impedance spectroscopy measurements of the samples were performed in a three electrode configuration with a Pt counter electrode and an Ag/AgCl KCl saturated reference electrode with a Bio-Logic SP-150 potentiostat with EIS capabilities. The AC impedance measurements were carried out in the dark in 1 M NaOH solution with a frequency range of 1 kHz to 1 Hz with AC amplitude of 25 mV and 5 min dwell time at every DC applied voltage point for stabilization.

3. Results and Discussion

The atomic composition of the samples as determined by inductive coupled plasma (ICP) mass spectroscopy is shown as a function of the atomic percentage of Al in the electrolyte deposition solution in Table 1. These data were used to determine the percentage of Al vs Al + Fe in the film as a function of Al in the electrodeposition electrolyte; the Al

Table 1. Atomic % of Al in Doped Samples Determined by ICP as a Function of % of Dopant in Electrodeposition Bath

solution Al (%)	ICP Al (%)	ICP Al STDEV (%)
0	0.01	0.01
6	0.38	0.21
10	0.46	0.02
20	1.47	0.12
25	3.14	0.04
30	4.67	0.16
35	7.91	0.00
40	9.99	0.11

concentration reported is that of the electrolyte unless otherwise indicated.

The scanning electron micrographs of the undoped and Al-doped samples, Figure 1, show evidence of significant morphological changes to the electrodeposited films with the addition of Al to the deposition bath. Figure 1(a) shows the morphology of the undoped sample, while Figure 1(b) shows the characteristic morphology of a sample with $\sim 0.45\%$ Al in the film deposited from 10% Al in the electrolyte which has very similar features to those of the samples deposited from solutions in the range of 6–20% Al in the electrolyte (0.37%–1.47% atomic in the film). The samples deposited from 6 to 20% Al in the electrolyte have features which are ~ 2 to 3 times larger than the undoped sample (0% Al). In contrast, when the electrolyte concentration reaches 40% Al ($\sim 10\%$ atomic Al in the film), Figure 1(c), the features of the sample are reduced and the structure is more densely packed than that of the undoped sample.

The grazing incidence ($\theta = 0.5^\circ$) X-ray diffraction (XRD) data were indexed to hematite (α -Fe₂O₃, space group: R3c (167), $a = b = 0.50356$, $c = 1.3748$ nm); the reference pattern used to index the peaks was JCPDS 33-0664. The reference α -Al₂O₃ pattern used was JCPDS 1-1296 (α -Al₂O₃, space group: R3c (167), $a = b = 0.50280$, $c = 1.3730$ nm). In the spectra, Figure 2(a), the crystallite sizes were obtained using the Scherrer equation on the near basal (104) reflection showing crystallites of ~ 49 nm for 0% Al, ~ 28 nm for 0.38% Al, ~ 69 nm for 0.46%, and 1.47% Al, and a reduction in size to ~ 24 nm for 10% Al substitution. At lower concentrations of Al doping the crystallite size is decreased; however, in the region of 3–5% aluminum-doping there is greater crystallinity with larger crystallites which then decrease in size at higher Al concentrations. This suggests that small concentrations of Al substituted in the octahedral position provide lattice strain relief. Similar effects have been observed by Schwertmann⁴⁵ in the FWHM of the XRD peaks as a function of Al in the hematite structure. Although the morphology shown on the SEM micrographs (Figure 1) indicates an increase in the particle size for the 1.48% atomic Al-doped sample and a decrease in particle size for the $\sim 10\%$ atomic Al-doped sample, all of the particle sizes shown in the SEM are between 50 and 150 nm which is consistent with multiple domains in each of the particles shown in the SEM micrographs. When the

(43) Jaramillo, T. F.; Baeck, S. H.; Kleiman-Shwarscstein, A.; McFarland, E. W. *Macromol. Rapid Commun.* **2004**, 25, 297.

(44) Jaramillo, T. F.; Baeck, S. H.; Kleiman-Shwarscstein, A.; Choi, K. S.; Stucky, G. D.; McFarland, E. W. *J. Comb. Chem.* **2005**, 7, 264.

(45) Schwertmann, U.; Fitzpatrick, R. W.; Taylor, R. M.; Lewis, D. G. *Clays Clay Miner.* **1979**, 27, 105.

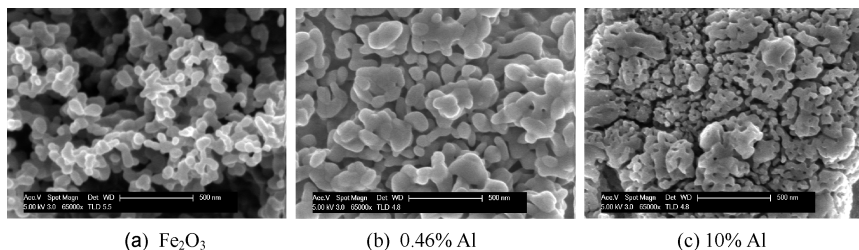


Figure 1. SEM of selected samples (a) Fe_2O_3 , (b) 0.46% Al, and (c) 10% Al dopant in the hematite film as characterized by inductive coupled plasma.

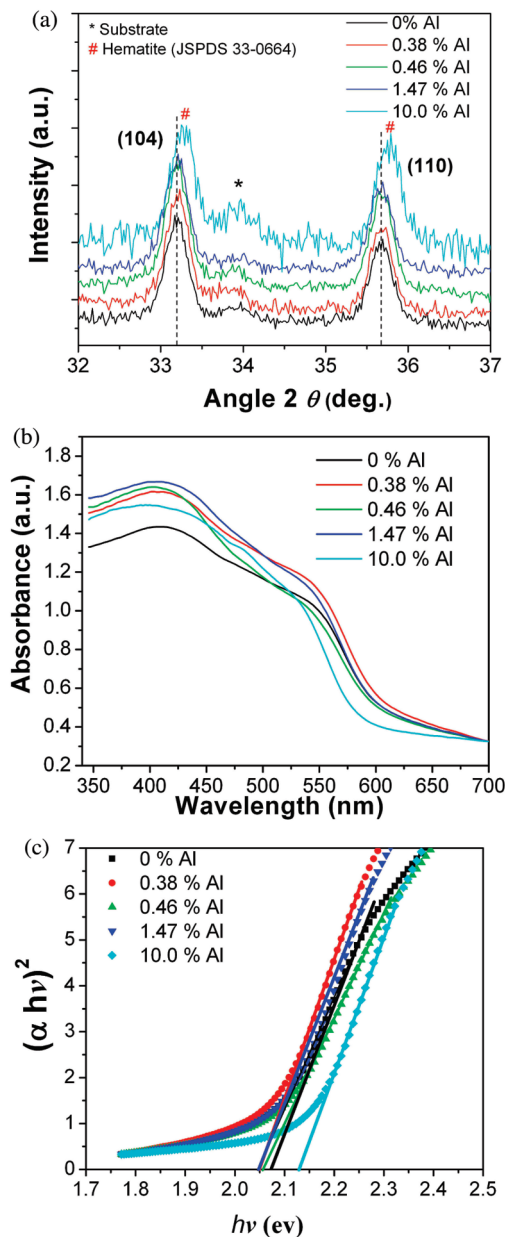


Figure 2. (a) XRD, (b) UV-vis, and (c) Tauc-Plots of undoped and Al-doped hematite thin film samples.

dopant concentration is increased to $\sim 10\%$, a clear shift of peak position toward higher angles is observed as compared to the spectra obtained for the samples with lower Al concentrations (1.48% to 0% Al). The Vegard's

lattice parameter rule⁴⁶ would show a linear decrease of the lattice parameter as a function of Al substitution with a change in the lattice constant from 5.0356 to 5.03484 Å (utilizing Vegard's rule) when substituted with 10% Al; a deviation from this rule has been shown by Schwertmann⁴⁵ in which he experimentally observed a shrinkage of $\sim 0.3\%$ in the lattice constant when substituted with 10% Al. Similar effects have also been observed for ferrihydrite when doped with aluminum.⁴⁷ This observation is consistent with a decrease in the unit cell volume expected from the substitution of the relatively small aluminum atom for the relatively large iron atom in Fe_2O_3 . Both peak broadening and a peak shift are observed for this sample possibly due to nonuniform strains in the lattice which would be expected by the substitutional nature of the aluminum-doping.

The UV-vis spectra of the samples are shown in Figure 2(b) and show minimal differences in the absorbance of the undoped and Al-doped films which are most likely attributable to difference in morphology observed by electron microscopy which change the scattering and internal reflection of the films (see Figure 1). The data are normalized to 700 nm to account for the scattering differences between samples. The UV-vis data were used to construct a Tauc-Plot (Figure 2(c)) with a fit to the data consistent with a direct bandgap of approximately 2.05 eV, which we have also previously observed for other dopant species in iron oxide.¹⁹ The aluminum-doping does not significantly modify the optical properties of the hematite thin films until the Al concentration is increased to approximately 10%. The absolute absorbance and the photoelectrochemical performance could be quantitatively decreased due to morphological differences in the electrodeposited films of different Al concentrations (Table 1). At an Al dopant concentration of $\sim 10\%$, there are modest changes in the spectrum, and the bandgap obtained from the direct gap fit increases from 2.05 to ~ 2.15 eV which may be the manifestation of the lattice strains observed in the XRD data.

The photoelectrochemical performance of the samples is shown in Figure 3. Under constant illumination, the J-V relationships are shown in Figure 3(a) for the hematite photoelectrodes deposited with varying amounts of Al in the electrolyte. The data are shown together with reference data from an undoped film in the dark. No changes were observed on the dark J-V relationships as a function of Al doping (data not shown), with the exception of

(46) Cox, A.; Sangster, M. *J. L. J. Phys. C: Solid State Phys.* **1985**, L1123.

(47) Jentzsch, T. L.; Penn, R. L. *J. Phys. Chem. B* **2006**, 110, 11746.

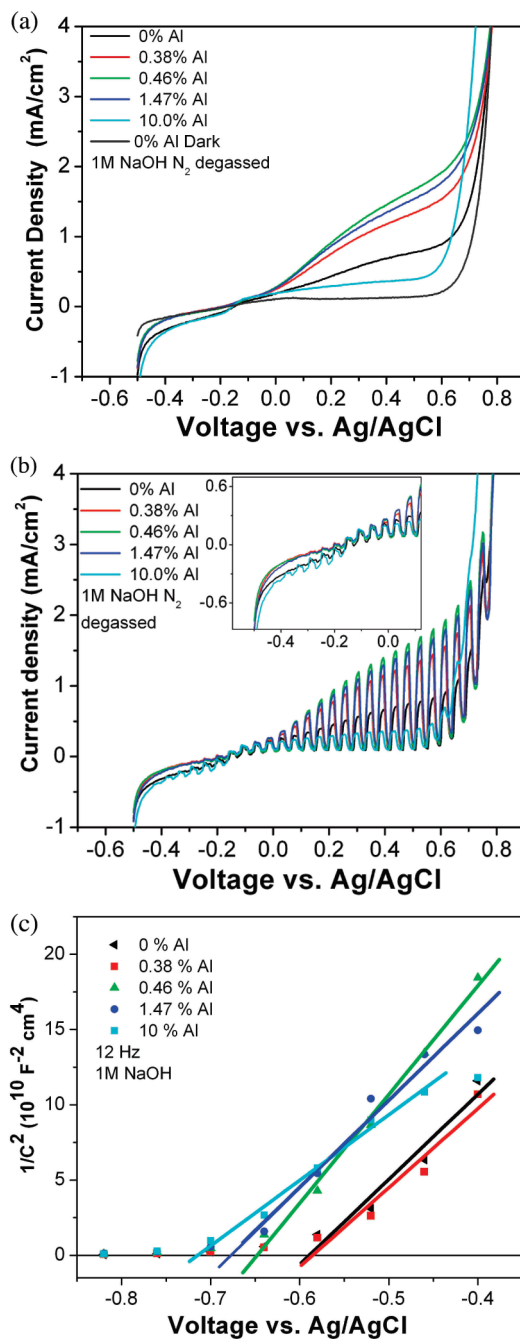


Figure 3. (a) J-V curves of the undoped and Al-doped photoelectrodes during illumination and 0% Al doped sample in the dark. (b) Chopped light J-V curve and inset of low applied voltage region. (c) Mott-Schottky at 12 Hz. All measurements are performed in N₂ degassed 1 M NaOH.

10% Al doped sample which shows a shift of ~90 mV in the electrochemical oxygen evolution potential as compared to the other samples. From this graph, an approximately 2-fold increase in the performance between the undoped sample and the 0.46% Al doped sample was observed. The PEC performance is increased showing a maximum at approximately ~0.5% dopant concentration (intermediate point corresponding to 2% Al in the electrolyte is not shown). Relatively small variations in the performance are observed for samples deposited with higher concentrations of Al. An example of an ~1.5% Al-doped hematite film is shown in Figure 3(a). At higher concentrations of Al in the

sample the performance is decreased and it can be seen that at 10% Al in the hematite film the photoelectrochemical performance decreases significantly. Chopped light J-V curves are shown in Figure 3(b) from this figure, a 2-fold improvement in performance for samples of up to 1.47% Al in the sample, can be seen. The photocurrent onset potential in the inset of Figure 3(b) is ~−0.3 V vs Ag/AgCl for all the samples with the exception of the 10% Al-doped sample has the photocurrent onset potential at ~−0.42 V vs Ag/AgCl which is shifted approximately −120 mV as compared to the other samples. This effect might be related with the early onset potential for oxygen evolution due to an applied potential (see Figures 3a and b in the region of 600–700 mV vs Ag/AgCl).

The flat band potential obtained from Mott–Schottky analysis in 1 M NaOH (Figure 3(c) for MS data at 12 Hz) was obtained in the range of 1 kHz to 1 Hz and the frequency dispersion of the flatband potential was ±20 mV. The averaged flatband potentials obtained were −624, −615, −660, −708, and −742 mV for the undoped 0.38, 0.46, 1.47, and 10% Al doped samples, respectively. The shift in the flatband potential of ~−100 mV to more negative values for the 10% Al doped sample is consistent with observation of the photocurrent onset potential shift. This shift can be explained by an increase in the bandgap of this highly doped sample by approximately 0.1 eV as shown from the Tauc Plot, Figure 2(c). All samples were observed to have flat band potentials more negative than the photocurrent onset potential which suggests a high recombination rate and kinetic hindrance on the hematite surface which would likely benefit from a surface catalyst. The photocurrent onset potential of the other samples was not observed which is probably due to the signal-to-noise ratio and the chopping frequency of the JV curve. The majority carrier donor concentrations (N_D) carriers/cm³ calculated from the Mott–Schottky analysis with E_0 12.5⁴⁸ are all in the range of 4×10^{21} to 7×10^{21} cm^{−3} for the 0–1.47% Al doping and 1.3×10^{22} cm^{−3} for the 10% Al sample; variations on N_D are attributed to changes in the electrochemically active area which rise from the electrodeposition process and are not accounted for by the geometric area. Therefore, the majority carrier donor concentrations are slightly higher than that reported for other hematite thin films 10^{20} – 10^{21} cm^{−3}.⁴⁹ Previous work on doped iron oxide has shown that with Pt¹⁶doped photoanodes there is a positive shift in the onset potential ~0.1 V as compared to the undoped hematite sample, and in systems doped with Cr and Mo¹⁹ no changes in the onset potential were observed.

The decrease in the photocurrent at high Al doping content could be related to the segregation of alumina to the surface (the largest Al concentration in a $\text{Fe}_{2-x}\text{Al}_x\text{O}_3$ solid-solution is 9 atomic % at 800 °C;⁵⁰ although

- (48) Schreblér, R.; Llewelyn, C.; Vera, F.; Cury, P.; Muñoz, E.; del Rio, R.; Meier, H. G.; Cordova, R.; Dalchiele, E. A. *Electrochim. Solid State Lett.* **2007**, *10*, D95.
- (49) Wilhelm, S. M.; Yun, K. S.; Ballenger, L. W.; Hackerman, N. *J. Electrochem. Soc.* **1979**, *126*, 419.
- (50) FactSage-Database.

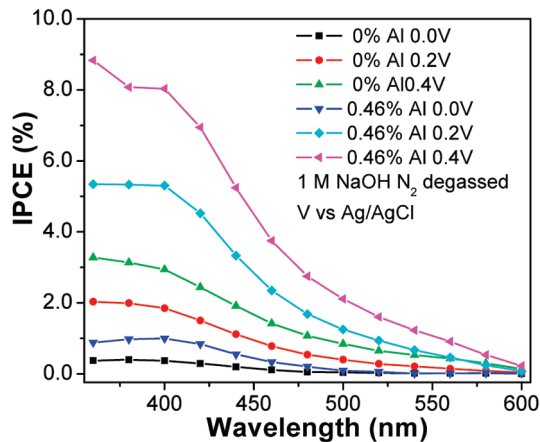


Figure 4. IPCE of selected samples at 0.2 and 0.4 V vs Ag/AgCl in N_2 degassed 1 M NaOH.

Schwertmann⁴⁵ and Muan⁵¹ has reported up to 15–18% Al incorporation in synthetic hematite. Alumina was not observed by XRD possibly due to a lack of crystallinity; however, it would be expected that alumina would segregate to grain boundaries or the surface of the hematite film creating a barrier for interparticle electron transport or from the electrolyte to the semiconductor. It has been reported that Al(OH)_3 segregating to the surface of aluminum-doped hematite and that these species were stable in mild NaOH treatments and 5 M NaOH at 70 °C for 1 h;⁴⁵ similar stability of the Al segregated species could be present in the highly doped hematite samples during testing in 1 M NaOH electrolyte. No change in the photoresponse of the 10% Al-doped sample was observed after pretreating for 24 h in 1 M NaOH in the dark following the initial testing. Although extended runs are planned in the future, the Al-doped samples have not shown decay in the performance in 1 M NaOH. The formation of Al species on the surface of the sample could be shifting the photocurrent onset potential as observed by both the photocurrent and Mott–Schottky onset potential.

The IPCE of the sample deposited from the 10% electrolyte (0.46% Al in the film) which has the best performance in comparison to the undoped sample is compared to that of the undoped film in Figure 4. From this figure it can be seen that a 2- to 3-fold improvement over undoped control samples at 0.46% Al substitution is observed which can be ascribed to changes in the electronic properties of the aluminum-doped films. The maximum IPCE that has been achieved on the optimized aluminum-doped sample is ~8% at 400 nm and 0.4 V vs Ag/AgCl. Although the absolute IPCE of the Al doped samples is low, there was a significant improvement in the IPCE in the doped samples, and LDA-DFT calculations were used to better understand the role of the isovalent doping. Differences between the shape of the UV–vis absorption (Figure 2(b)) and the IPCE (Figure 4) are related to the differences in absorption depth for photons of low energy compared to those of higher energies.

The low energy photons are absorbed further from the solid–liquid interface and holes produced must travel further to the electrode surface than the holes produced from photons with higher energy which are absorbed closer to the solid–liquid interface. The shorter transport distance is associated with a lower probability of recombination (Note that it has been reported that in the case of a hematite electrode the hole diffusion length is less than 5 nm⁵²).

First principle calculations with density functional theory (DFT) provide fundamental understanding of materials from electronic structure point of view. Local density approximation⁵³ to density functional theory (LDA-DFT), implemented in Vienna ab initio simulation package (VASP 4.6.21)^{54,55} was utilized to model the effects of doping on the hematite electronic structure. Plane wave cutoff energy of 400 eV was used and the ion positions and volumes of the supercells were always relaxed until the force on each of them is 0.01 eV or less. It is known from neutron diffraction study⁵⁶ that $\alpha\text{-Fe}_2\text{O}_3$ shows antiferromagnetic (AFM) behavior. We have also found that the antiferromagnetic (AFM) ordering in $\alpha\text{-Fe}_2\text{O}_3$ is important to consider in obtaining the ground state electronic structure. For this a larger hexagonal unit cell was chosen (with 12 Fe and 18 O atoms), and a layer-by-layer AFM order was found to be the preferred one. Our calculated band gap was 1.72 eV with DFT+U method with $U = 5.5$ eV. This value of U was chosen to optimize both the calculated band gap and the lattice constant. Our calculated lattice constants for the conventional hexagonal cell are $a = 4.925 \text{ \AA}$ and $c = 13.455 \text{ \AA}$, whereas the experimental values⁵⁷ are $a = 5.035 \text{ \AA}$ and $c = 13.754 \text{ \AA}$. Although an increase in U increases the band gap, it decreases the cell volume; however, the choice of U gave reasonable values for the both.

From the band structure (Figure 5(a)), the conduction band minimum (CBM) was found to be almost dispersionless due to the higher contribution from Fe-3d orbitals indicating a very high electron effective mass. The valence band maximum (VBM) shows little more dispersion due to the presence of more delocalized O-p contributions. Here, although the p-d optical transition is not forbidden, the photoconductivity would be expected to be low because of the low mobility of the electrons. With one aluminum atom replacing an iron atom in the supercell, there are only minimal changes to the band gap and band edge energies, Figure 5(b). The theoretical band gap of undoped $\alpha\text{-Fe}_2\text{O}_3$ was found to be 1.72 eV whereas the calculated band gaps for Al-doped $\alpha\text{-Fe}_2\text{O}_3$ are 1.71 eV and 1.69 eV for spin up and down channel, respectively. Figures 5(c) and 5(d) shows the partial density of states for undoped and aluminum-doped

- (52) Kennedy, J. H.; Frese, K. W. *J. Electrochem. Soc.* **1978**, *125*, C160.
- (53) Perdew, J. P.; Zunger, A. *Phys. Rev. B* **1981**, *23*, 5048.
- (54) Kresse, G.; Furthmüller, J. *Comput. Mater. Sci.* **1996**, *6*, 15.
- (55) Kresse, G.; Furthmüller, J. *Phys. Rev. B* **1996**, *54*, 11169.
- (56) Shull, C. G.; Strauser, W. A.; Wollan, E. O. *Phys. Rev.* **1951**, *83*, 333.
- (57) Kück, S.; Werheit, H. *Non-Tetrahedrally Bonded Binary Compounds II*; Springer-Verlag: New York, 2000.

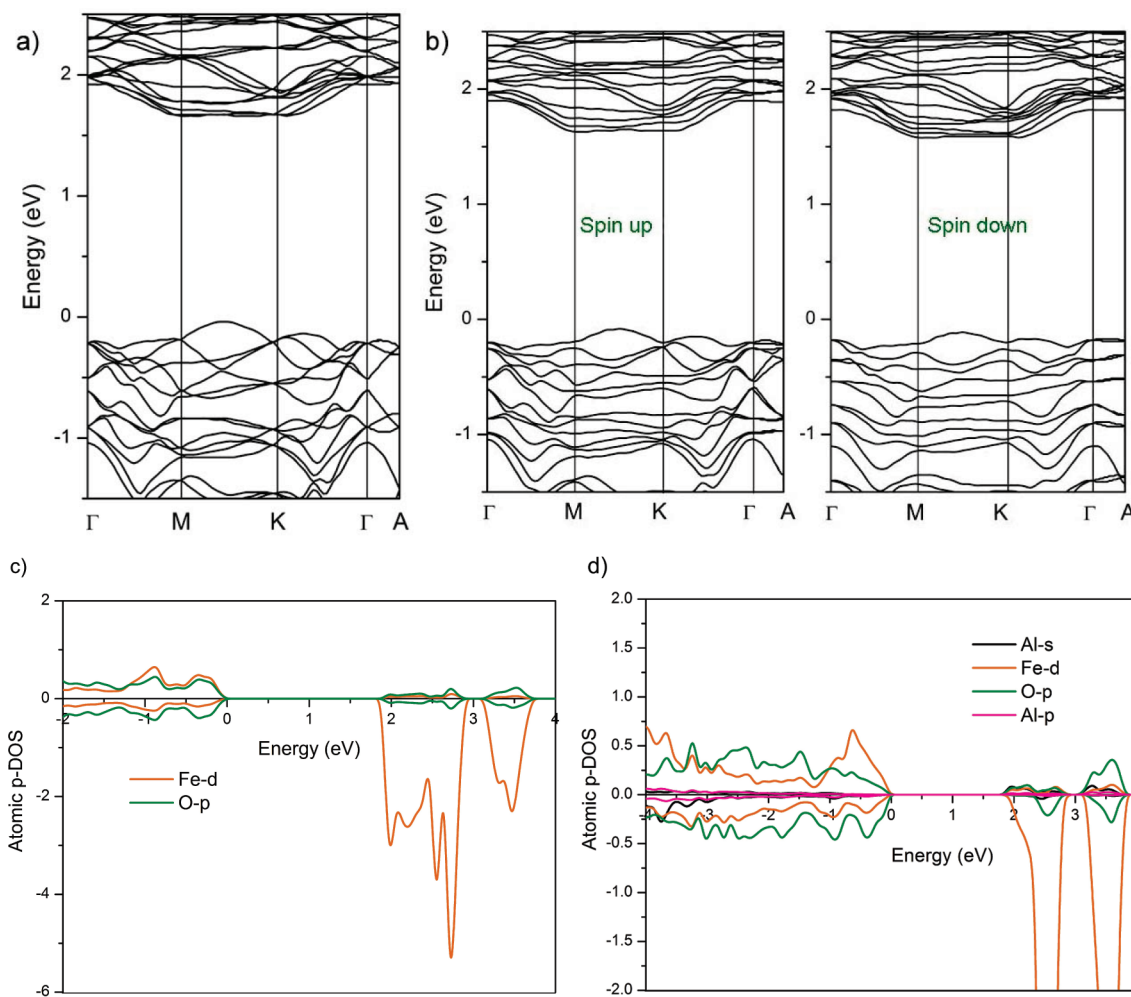


Figure 5. Band structure of (a) undoped α - Fe_2O_3 , (b) Al-doped α - Fe_2O_3 . Partial density of states (DOS) plots for (c) undoped α - Fe_2O_3 , (d) Al-doped α - Fe_2O_3 .

α - Fe_2O_3 , respectively, and suggest that the isovalent Al does not make a significant contribution to the electronic structure around the band edges. This is expected given the band gap of Al_2O_3 is more than 6 eV. Similar results were found for Ga and In substitutions in α - Fe_2O_3 . Overall, for all the group IIIA elements doped into α - Fe_2O_3 little change in the electronic structure is expected and conduction is expected to remain dominated by polarons.

The observed increase in conductivity from group III dopants in Fe_2O_3 can be explained due to the strain introduced in the lattice due to the small size difference of the dopant. Figure 6 shows the DFT calculated volume changes in Fe_2O_3 due to group III element doping. For In doping the volume increases compared to the undoped α - Fe_2O_3 . For polaron conduction, this is not favorable as the carrier hopping is hindered due to increased cation–cation distances. On the other hand, aluminum-doped α - Fe_2O_3 has a smaller volume than undoped α - Fe_2O_3 with a decrease in the Fe–Fe separation distance; hence Fe-d wave-function overlap would be increased and facilitate carrier hopping. Also shown in Figure 6, B doping in α - Fe_2O_3 would result in a greater volumetric distortion; however, due to the large size mismatch between Fe and B the solid solution would likely not be

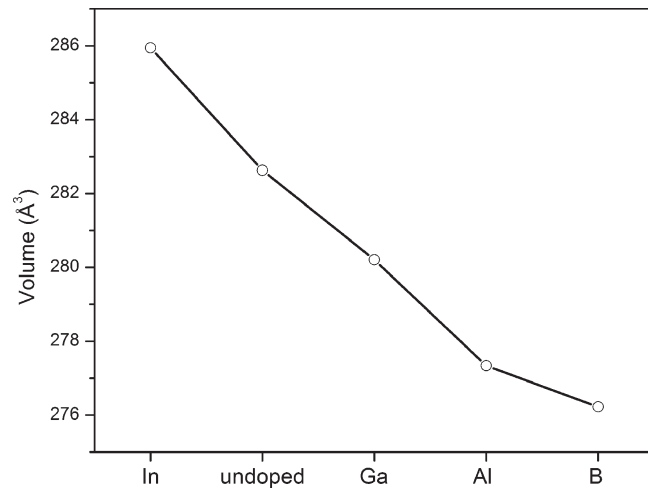


Figure 6. Group IIIA element doped α - Fe_2O_3 and their calculated volumes are shown.

stable. Unfortunately, doping of any Group IIIA element into hematite would not alter the basic conduction mechanism of small polaron hopping; although aluminum-doped α - Fe_2O_3 would be expected to have a better photoresponse than the undoped α - Fe_2O_3 , by virtue of the unchanged optical properties and small increase in strain induced conductivity, no dramatic increase in

photoresponse would be expected. The observed increase in IPCE of the 2- to 3-fold over the undoped material is consistent with this theoretical interpretation.

4. Conclusions

We have shown that the Group IIIA element, aluminum, can be electrochemically doped into hematite thin films. The Al concentration in the sample can be controlled by modification of the dopant concentration in solution showing the best relative photoelectrochemical performance from a hematite film doped with 0.46 ± 0.02 atomic % Al deposited from an electrolyte with 10% dissolved Al. Higher concentrations of Al in the film had a detrimental impact on the photoelectrochemical properties of the hematite photoanodes possibly due to phase segregation of Al at the grain boundaries of the film. LDA-DFT calculations have shown that when an aluminum atom replaces an iron atom (aluminum-doping) in the conventional unit cell, there are only

minimal changes to the band gap and the band edges remain nondispersive. This would suggest that the iso-valent Al does not make a significant contribution to the electronic structure around the band edges. We interpret the higher PEC performance to be due to the increase conductivity of the hematite associated with the strain introduced in the lattice due to the aluminum substitution for iron.

Acknowledgment. Funding was provided by the DOE Hydrogen Program (DEFG36-05GO15040) with partial support from the National Science Foundation (MRSECDMR05-0415). The work made use of the UCSB Nanofabrication Facility (NSF-funded NNIN). We thank Mr. Robert Norton for technical assistance and Drs. Siqi Shi and Chuying Ouyang for their valuable suggestions. The work at NREL was supported by the DOE under Contract DE-AC36-08GO28308. This research used computational resources at NERSC which is supported by the Office of Science, DOE, Contract No. DE-AC36-08GO28308.